Electron Detachment and Relaxation of OH^-(aq)

Christian Petersen, Jan Thøgersen, Svend Knak Jensen, and Søren R. Keiding*

University of Aarhus, Langelandsgade 140, DK-8000, Aarhus C, Denmark

Received: June 12, 2007; In Final Form: August 16, 2007

Femtosecond transient absorption spectroscopy is used to study the primary reaction dynamics of photoinduced electron detachment of the hydroxide ion in water, OH^- (aq). The electron is detached by excitation of OH^- (aq) to the charge-transfer-to-solvent (CTTS) state at 200 nm. The subsequent relaxation processes are probed in the spectral range from 193 to 800 nm with femtosecond time resolution. We determine both the time-dependent quantum yields of OH^- (aq), OH(aq), and e^-(aq), and we observe a transient spectral signature which is assigned to relaxation of hot $(OH^-)^*$ ions formed via solvent-assisted conversion of the excited CTTS state to OH^-. The primary quantum yield of OH(aq) is 65 ± 5%, while recombination with e^-(aq) reduces the yield to 34% after 5 ps and 12% after 200 ps. The yield of hot $(OH^-)^*$ ions is 35 ± 5%. Rotational anisotropy measurements of OH^- (aq) and OH(aq) indicate a reorientation time for OH^- (aq) of 1.9 ps, while no rotational anisotropy is resolved for the OH(aq) radical within our time resolution of 0.3 ps. This is consistent with the notion that OH(aq) radicals formed after electron detachment are only weakly bound to the hydrogen bond network of water. The assignment of the experimental data is supported by a series of electronic structure calculations of simple complexes of OH^- $(H_2O)_n$.

1. Introduction

The detachment threshold of the isolated hydroxide ion, OH^- $(X^1\Sigma)$ is 1.83 eV.[1,2] In aqueous solution the surrounding water molecules stabilize the OH^- (aq) ion and approximately 9.2 eV are needed to detach the electron into vacuum.[3] However, the energy needed to liberate the electron from OH^- (aq) to form a hydrated electron is lower. Thus, exciting the charge transfer to solvent band of OH^-(aq), peaking at 6.6 eV,[4] will generate hydrated electrons. This brings the aqueous detachment energy to, and slightly above, the onset of indirect ionization of pure liquid water, starting approximately at 6.5 eV.[5] Based on the proximity of the ionization threshold of water, and the spectral properties of the OH^-(aq) absorption band, the detachment of the electron from OH^- (aq) is believed to proceed through a short-lived charge-transfer-to-solvent (CTTS) state in a mechanism similar to the mechanism for photodetachment of halide ions in water.[6] The electron in the CTTS state is quasi-bound by the potential from lingering water molecules reminiscent of the hydration of ground state OH^-(aq). Solvent fluctuations rapidly cause the electron to be adiabatically released from the CTTS state and a complex, or contact pair, $(OH:e^-)_{aq}$ is formed.[7,8] We will in the remaining part of the paper omit the (aq) postfix and assume that all species are hydrated unless explicitly stated. The exact nature of the CTTS state and the contact pair have been debated intensely during the last 10 years in an effort to understand the diverse experimental and theoretical results. In particular quantum yields of free hydrated electrons and contacts pairs, and their subsequent geminate recombination dynamics, have been investigated in the halide ions F^-, Cl^-, and I^-.[8−13] Direct experimental evidence for both the CTTS state and the contact pair are elusive for the aqueous halide and pseudohalide ions. The lifetimes of the CTTS states fall in the range of the experimental time resolution of femtosecond experiments and are difficult to observe due to the presence of intense coherence spikes around $t = 0$. Furthermore, the spectrum of the electron in the contact pair closely resembles that of the free hydrated electron.[14] The separation of OH and e^- in the contact pair, and whether solvent water molecules separate the pair, is unknown. However, the observation of a bimodal recombination dynamics composed of a fast ∼2 ps recombination of $OH:e^-$ in close contact and a slower ∼30 ps recombination of separated freely diffusing OH and e^- pairs, demonstrates that the recombination dynamics following photodetachment of aqueous OH^- cannot be described without an attractive mean force potential acting between OH and e^- products. The attractive potential of the $OH:e^-$ contact pair is only 2−3 kT.[8] The contact pair therefore readily breaks apart forming the isolated species of OH and e^-. The experimental observation of hydrated electrons 0.4 ps after the excitation of OH^- thus indicates an upper limit for the lifetime of the CTTS state.[7] As a result of the large diffusion coefficients of the two fragments, the attractive mean force potential, and the tight ejection distribution, a large fraction of the hydrated electrons recombines with the geminate OH radicals. Using photometric measurements and ultrafast actinometry, Sauer et al.[11] have determined the photodetachment quantum yield of QY(5ps) = 34 ± 8% after 5 ps and estimated the prompt and free electron yield to QY($t \rightarrow 0$) = 37% and QY ($t \rightarrow \infty$) = 9%, respectively. The free electron yield is in good agreement with the QY = 11% measured by Dainton and Fowles[15] at 185 nm, and Iwata et al.[16] and Sauer et al.[11] using an excitation wavelength of 193 nm.

In the present work we use femtosecond transient absorption spectroscopy to study the primary reaction dynamics of the photoinduced electron detachment of OH^- following closely the work of Crowell et al.[8] A 200 nm pump pulse initiates the detachment and the resulting photoproducts are monitored by probing their time-dependent absorption in the spectral range from 193 to 800 nm. We measured the transient absorption the

* Author to whom correspondence should be addressed. E-mail: thogersen@chem.au.dk.

10.1021/jp0745438 CCC: $37.00
Published on Web 10/16/2007

first 20 ps for all probe wavelengths and to 200 ps at selected wavelengths. The complete coverage of the spectral region where the possible products absorb enables direct observation of transient species and possibly any spectral dynamics reflecting the relaxation or hydration of the photoproducts. In addition, it also allows for the determination of the time-dependent quantum yields of OH^-, OH, and e^-. As mentioned above, the notion of electron detachment through a short-lived CTTS state and the existence of the weakly bound contact pair is based on the spectral shape of the OH^- absorption band[17] and the subsequent time evolution of the $OH+e^- \rightarrow OH^-$ geminate recombination.[7,8] A delayed appearance of the detachment fragments indicating a finite upper state lifetime would further support this assignment. However, so far only an upper value of its lifetime has been derived from the appearance of the hydrated electron absorption. The exact time for the detachment of the electron is vitiated with some uncertainty, as its absorption spectrum undergoes substantial changes during hydration. Furthermore, the involvement of the $OH:e^-$ contact pair in the detachment process rests on theoretical considerations and the fact that the recombination dynamics cannot be explained from free diffusion alone. By probing the hydroxide ion, the hydroxyl radical and the hydrated electron we seek further information on the CTTS state and the contact pair.

We have, for characteristic wavelengths, also measured the rotational anisotropy of the fragments. The rotational anisotropy of OH^- and OH may show if the orientation of the excited OH^- molecules is transferred to the OH fragment and thereby elucidate the processes between the excitation of OH^- and the actual electron detachment. Small halide ions in water clusters are known to have well-defined hydration structures as a result of strong hydrogen bonds to nearby water molecules.[17] Strong hydrogen bonds could give rise to detectable rotational anisotropies as a results of the slow reorientation of water molecules.[18]

The paper is organized as follows: Section 2 introduces the absorption spectra used to identify the species involved in the photodetachment. The femtosecond transient absorption spectrometer is described in section 3, while section 4 presents the experimental results. Section 4 is divided into three subsections. Section 4a identifies the end products of the photodetachment and describes their time evolution. Section 4b describes a short-lived intermediate species, while section 4c reports the rotational anisotropy of OH^- and of the photoproducts. The experimental results are discussed in sections 5a−c. Section 5a presents a kinetic model based on solving the diffusion equation for the geminate partners under the influence of a weakly attractive potential. This leaves a small residual absorption, which is assigned to hot $(OH^-)^*$ molecules relaxing toward the ground state of OH^-. In section 5b we compare the model from 5a to the rotational anisotropies observed at different wavelengths for OH^- and OH. Section 5c is a theoretical section where we discuss the result of high level *ab initio* calculations of small $[OH^-:n(H_2O)]$ clusters in light of the experimental observations presented. The paper concludes by summarizing the consequences of the experimental findings.

2. Absorption Spectra

This section presents the steady-state absorption spectra of OH^-, OH, and the hydrated electron, e^-. As several spectra have been reported for each species, and since our modeling of the observed dynamics depends of our choice of which steady-state spectra are used, we will describe the spectra in detail. The spectrum of OH^- depicted in Figure 1a shows an absorption peaking below 193 nm and dropping off to zero at around 220 nm. The absorption spectrum of OH has been measured by Pagsberg et al.,[19] Thomsen et al.,[20,21] Boyle et al.,[22] Czapski et al.,[23,23] Alam et al.,[24] and recently by Janik et al.[25] The spectra shown in Figure 1b are in fair agreement for wavelengths longer than 230 nm. However, below 230 nm the spectra deviate significantly ranging from the sharp declining absorption measured by Czapski et al.[23] to the steady increase observed by Alam et al.[24] None of the measured spectra cover the spectral range probed in the present measurements, and we have therefore extrapolated the measured spectra down to 193 nm. However, at 193 nm the extinction coefficients resulting from the extrapolation of the various curves deviate by ∼500 L/mol cm, and the conclusions derived from fitting the kinetic models to the data must therefore be interpreted with this in mind. However, as will be shown later, the OH spectra that drops toward lower extinction below 200 nm gives the best agreement with the experimental data presented here.

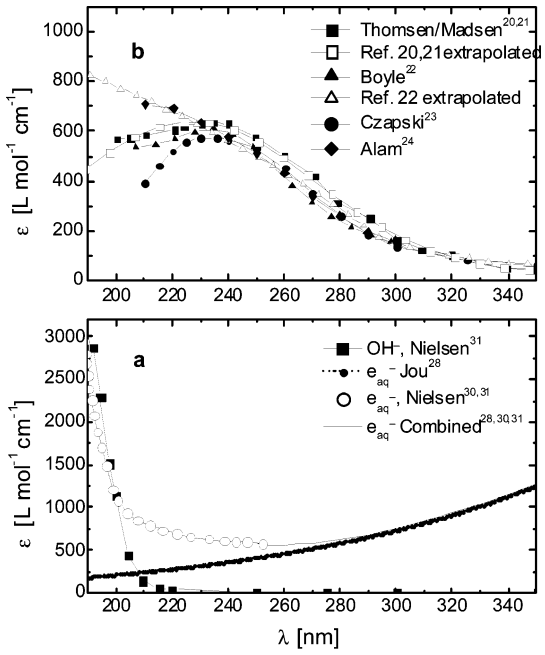

Figure 1. Equilibrated absorption spectra of (a) OH^-[31] and e^-.[28,28,30,31] (b) Equilibrated absorption spectra of OH reported by Thomsen/Madsen et al.[20,21] Boyle et al.,[22] Czapski et al.[23] together with the spectra of Thomsen/Madsen and Boyle extrapolated to 193 nm.

Numerous authors have measured the absorption spectrum of the hydrated electron,[26−29] but only Nielsen et al.[30,31] measured the spectrum at far-UV wavelengths, covering the range from 200 to 250 nm. We have used the combined hydrated electron spectra of Nielsen et al.[30,31] and Jou and Freeman[28] throughout the analysis. Notice that the absorption of the hydrated electron increases below 210 nm. The microscopic origin of the far-UV spectrum of the hydrated electron was recently investigated by Shkrob et al.[32] On the basis of calculations on small anionic water clusters, they suggested that the UV transition is related to an electronic transition in the first solvation shell of water molecules surrounding the hydration site of the electron. No spectral signatures above 200 nm are reported in literature for hydrated cations in accordance with our observations. Given the experimental uncertainty, to be discussed below, and the uncertainty of the reported spectra, we allow for at 5−15% variation in amplitude of the steady state absorption spectra.

3. Experimental Setup

The double-beam transient absorption spectrometer utilized in this work is similar to the one used in a previous study.[33,34]

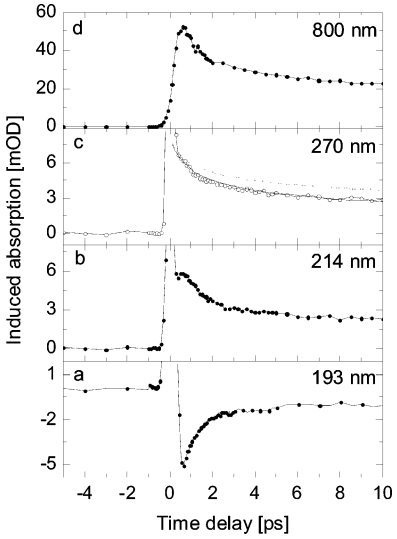

Figure 2. Transient absorption dynamics at (a) 193, (b) 214, (c) 270, and (d) 800 nm. The $t = 0$ peak has been truncated for clarity. The dashed and the dotted lines in c are two different recombination models with and without a weak attractive potential between the two fragments. This is discussed in detail in section 5b.

Briefly, a 1 kHz titanium−sapphire laser system emitting 100 fs pulses with pulse energy of 0.75 mJ is frequency quadrupled to generate the 200 nm pulses. The pump pulse is focused through the sample by a $f = 50$ cm concave mirror and the energy is $\sim 6\ \mu$J. A two-stage optical parametric amplifier (OPA) pumped at 400 nm generates the probe pulses across the spectral range from 460−800 nm. Probe pulses ranging from 230 to 460 nm are produced by frequency doubling, while the spectral region between 193 and 300 nm is covered by frequency mixing the OPA pulses with either 400 nm or 266 nm pulses. The probe beam is focused onto the sample by an $f = 5$ cm CaF_2 lens. The polarization of the pump pulse is at the magical angle (54.7°) relative to the polarization of the probe pulse. For the measurements of the rotational anisotropy the pump and probe pulses are either polarized parallel (∥) or perpendicular (⊥) to one another.

The sample consists of a ∼0.15 mm thick jet of 40 mM KOH in aqueous solution. The flow is adjusted to give a fresh sample for every laser pulse. The reproducibility of the transient absorption data is tested among consecutive scans as well as by repeating the measurements on different days using different samples. The transient absorption spectrum is measured on a common absorption scale with an uncertainty across the entire spectrum of ±15%. The dominant contribution to this uncertainty stems from small variations in the diameter of the probe beam and the effect is minimized by keeping the pump beam cross section (∼150 μm) much larger than that of the probe beam (<∼60 μm). A separate set of measurements covering the entire spectral range at a fixed delay of 10 ps is measured with high accuracy, and the common absorption scale of the transient absorption data, shown as a contour plot in Figure 3, is constructed by scaling the individual transient absorption traces to the accurately determined transient absorption spectrum at 10 ps. We note that this procedure accurately reproduces the well-known spectrum of the hydrated electron at visible and NIR-wavelengths.

4. Experimental Results

4a. Description of the Transient Data. Figure 2a−d shows selected wavelengths of the transient absorption spectrum from 193−800 nm induced by the 200 nm pump pulse. All measurements are taken at magic angle (54.7°) in order to avoid orientation effects in the absorption transients. Below approximately 400 nm, all curves display an initial sharp peak resembling that obtained at the same wavelength when neat water is replaced for the OH^- solution. However, the width of the $t = 0$ peak is at some wavelengths significantly longer than that observed in neat water, indicating an early appearance of the photodetachment products. We assign the $t = 0$ peak in neat water to coherent two-photon absorption in water[35] and take the temporal position and width to mark the point of zero delay and upper limit of the temporal resolution (0.3 ps), respectively. The data may be divided into three sections depending on the spectra of the species in play. The interval from 193 to 220 nm involves the absorption of OH^-, OH and e^-. The interval from 220−400 nm relates to the absorption of OH and e^-, and above 400 nm the absorption is entirely due to e^-. We have scanned the time delay to 200 ps for a number of probe wavelengths, but for clarity we only depict the data from −5 to 10 ps. Beyond 10 ps the data reveals nothing but the slow decay of the OH and e^- transient absorption and the recovery of the OH^- signal caused by diffusive geminate recombination, as we will discus below.

193−220 nm. The measurement obtained at 193 nm (Figure 2a), reflecting the absorption of OH^-, OH, and e^-, displays an initial negative absorption (bleaching) of −5.5 mOD caused by the excitation of the CTTS band of OH^-. The absorption recovers to a nearly constant level of −0.5 mOD on two distinctly different time scales. The majority of the absorption constituting ∼4 mOD recovers in 2 ps, while the remaining ∼1 mOD recovers in about 20 ps. Close inspection of the measurement at 193 nm reveals that the absorption recovery is in fact followed by a slight decrease after 3 ps, suggesting the presence of a transient absorption entity. This feature becomes more pronounced at wavelengths longer than 199 nm, as the contribution from OH^- decreases and the bleaching associated with the excitation of OH^- is replaced by an induced absorption rising in 0.5 ps and decaying on a 2 ps time scale. This is illustrated in Figure 2b showing the dynamics at 214 nm. Although the coherent spike somewhat masks the early time dynamics, a small dip can be observed after the large peak at $t = 0$, indicating the delayed growth of a positive transient signal.

220−400 nm. The transient absorption from 220 to 400 nm is caused by OH and e^-. The absorption dynamics is illustrated by the measurement taken at 270 nm in Figure 2c. At 270 nm the width of the $t = 0$ peak is 0.5 ps (fwhm), thus slightly broader than the estimated time resolution of 0.3 ps. This is indicative of an immediate appearance of at least some of the OH and e^- detachment products. It is immediately followed by a positive absorption of 5.5 mOD, which decays following a double exponential decay curve with time constants 2.2 ps (60%) and 30 ps (40%). The coherence peak completely dominates the first 0.5 ps thereby obscuring the onset of the absorption of OH and e^-. Hence, the absorption traces in this spectral region do not provide additional information of the OH^- CTTS state, apart from stating that the CTTS state in OH^- must have a lifetime shorter than ∼0.3 ps. The dashed and dotted lines are two different models, with and without an attractive potential, that describe the decay of the signal due to recombination of OH and e^-. The models will be discussed in detail in section 5.

400−800 nm. Above 400 nm the absorption is entirely due to the hydrated electron. The measurement at 800 nm displays an absorption peaking at 52 mOD after 0.5 ps. Within the uncertainty associated with the 0.3 ps temporal resolution of

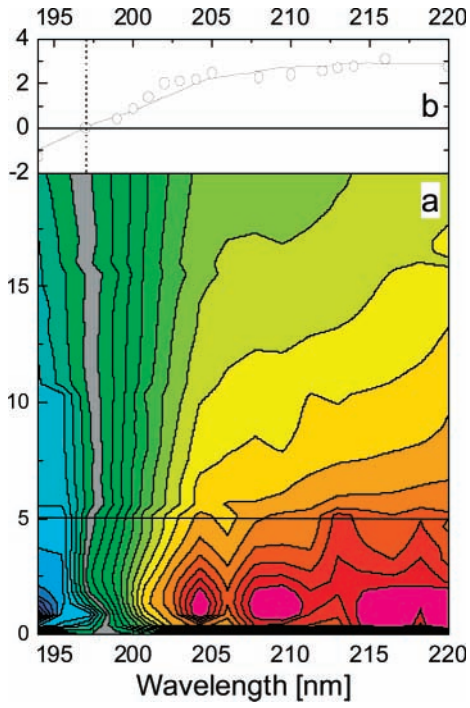

Figure 3. (a) Contour plot of the transient absorption from 193 to 220 nm following the photolysis of OH^- at 200 nm. We have colored the contour, $\Delta A = 0$ gray to emphasize the areas of negative transient absorption at shorter wavelengths (blue contours) and positive transient absorption above 200 nm (green and yellow contours). The scale goes from −3 mOD to +4 mOD. (b) Shows the transient spectrum at 5 ps and the spectrum obtained by adding equal contributions of OH^- (bleaching) and OH and e^- (induced absorption).

the experimental setup the early absorption dynamics of the detached electron is identical to that pertaining to the direct photoionization of water, when taking into account the slightly smaller ejection lengths of the electron caused by 1 photon excitation at 200 nm.[20,36] Hence, the data in this region do not, as for the region from 220 to 400 nm, reveal any new information concerning the existence of a spectrally distinct CTTS state or a delayed appearance of the detachment products. Again an upper limit for the lifetime of the CTTS state of 0.3 ps can be inferred from the experimental data. After $t = 0$ the absorption decays to a nearly constant level of 10 mOD following a time dependence identical to the 270 nm transient. The decay of the absorption above 400 nm pertaining to e^- also matches the recovery of the absorption below 200 nm associated with the slow (~20 ps) component of the recovery of the OH^- absorption after 2 ps. Accordingly, we conclude that the decay in the hydrated electron concentration is entirely dominated by recombination with OH. The measurement at 800 nm is in good agreement with the measurements recorded at 800 nm by Crowell et al.[7]

4b. The Short-Lived Transient. Figure 3a shows a pseudo 3D plot of the spectral range from 193−225 nm. The data around $t = 0$ have been truncated in order to reduce the dominating peak at $t = 0$. Figure 3b compares the transient spectrum after 5 ps to the total absorption of the equilibrated OH^-, OH, and e^-. We note that, for delays longer than 5 ps, an isobestic point is observed at 197 nm (dashed line) in accordance with the steady-state spectra of e^-, OH, and OH^-, thus corroborating that these species are the only contributors to the transient spectra observed after 5 ps. However, at delays shorter than ~4 ps, the transient spectra are poorly matched by any combination of equilibrated OH^-, OH, and e^- spectra. Nor can the spectra be assigned to any of the products from the photolysis of the water solvent.[20] Accordingly, we infer that transient species other than the equilibrated OH^-, OH, and e^- are present during the first ~4 ps. Referring again to Figure 3a, the measurements at wavelengths below 197 nm clearly show the negative absorption caused by photodetachment of OH^-. In contrast, the spectrum from 204 to 225 nm shows a positive transient absorption lasting about 2 ps. At 225 nm, this absorption appears immediately ($t < 0.5$ ps) after the excitation and disappears after 1.5 ps. As the wavelength becomes shorter, the absorption increases and its maximum moves toward longer delays before the absorption merges with the negative absorption pertaining to ground state of OH^- below 200 nm. The additional absorption transient is not due to short-lived excited states of OH, e^-, or OH^-. Halide ions are not expected to have excited states below their CTTS state, and nor do we see indications that this should be the case for OH^-.[37] As for OH, the excitation of OH^- at 6.2 eV populates the lowest lying CTTS band. The resulting OH fragment is in the $^2\Pi$ ground state, since the excited states of OH exceeds the available energy.[37] The absorption spectrum of ground state OH is incompatible with the spectrum of the short-lived transient and therefore excludes ground state OH as a candidate.

On the other hand, the short-lived transient absorption dynamics resemble the spectral behavior associated with the vibrational relaxation following recombination as previously observed in a number of small, hydrated molecules including CS_2, NO_3^-, I_2CH_2, and ClO_2,[33,38−40] where the absorption decays toward the band center with a decay time that becomes shorter and shorter as one moves away from the band center.[41] Also, spectral relaxation has been observed subsequent to the recombination of iodine atoms and electrons following photodetachment of I^-.[14] The fact that the spectral propagation approaches the equilibrated spectrum of OH^- and not that of OH suggests that the absorption pertains to excited OH^-. As we will discuss later, we are inclined to assign the short-lived transient to a conversion of the CTTS state into hot $(OH^-)^*$ molecules that subsequently relax to ground state OH^-. Internal conversion describes the process where electronic excitation energy is converted into vibrational energy through a nonadiabatic coupling between the electronic degrees of freedom and the intramolecular vibrational modes. In the present case the conversion process is very efficient due to the very strong coupling between the solvent and the solute, H_2O-OH^-, as well as the matching donor and acceptor vibrational frequencies making the relaxation very fast.[42] In addition, we note that the immediate (<0.5 ps) appearance of the short-lived transient suggests that the relaxing OH^- is formed by immediate geminate recombination of closely spaced OH:e^- pairs, or due to OH^- molecules undergoing direct solvent-assisted conversion from the CTTS state.

4c. Polarization Measurements. Information about the rotational motion of the species involved in the photolysis may be obtained from the rotational anisotropy:

$$r(t) = \frac{\Delta A_{\parallel} - \Delta A_{\perp}}{\Delta A_{\parallel} + 2\Delta A_{\perp}} \tag{1}$$

$r(t)$ is measured by probing the induced absorption with the probe polarized parallel, $\Delta A_{\parallel}$, and perpendicular, $\Delta A_{\perp}$, to the polarization of the excitation pulse. In order to measure the reorientation of a specific molecule, it is important that contributions to the absorption from other species are negligible. Because of overlapping absorption spectra, this requirement is fulfilled for neither OH^- nor OH. For the probe wavelengths

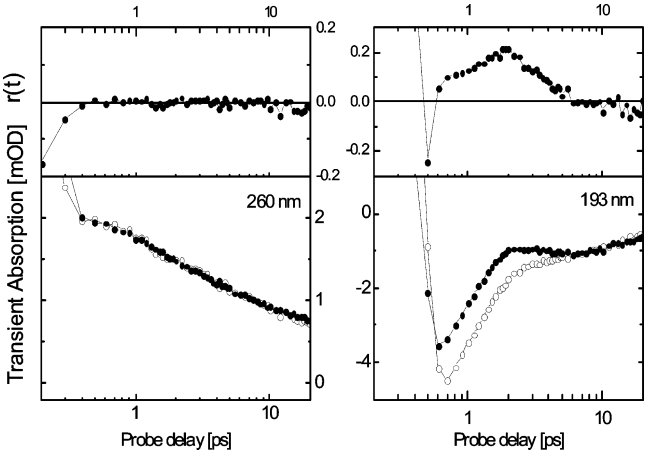

Figure 4. Rotational anisotropy measured at (a) 260 nm and (b) 193 nm together with the transient absorption traces at the two wavelengths. Note the logarithmic time scale.

accessible in our setup, the most favorable condition for OH^- is achieved by probing the absorption at 193 nm, where the extinction coefficient of OH^- is 5 and 1.25 times that of OH and the e^-, respectively. Whereas for OH, the best conditions are obtained at 260 nm, where only OH and e^- absorb and where the extinction coefficients of these two species are about the same. The equilibrated hydrated electron has no rotational anisotropy after 5 fs,[29] and any rotational anisotropy in the transient absorption at 260 nm thus stems from the OH fragments. Figure 4a shows the rotational anisotropy of the OH radicals represented by the measurement at 260 nm. Since the strong $t = 0$ transients are very different for parallel and perpendicular polarizations of the beams, the determination of $r(t)$ within the first 0.3 ps is inaccurate. After 0.3 ps there is no rotational anisotropy. Consequently, the orientation of OH radicals emanating from the detachment process is isotropic after 0.3 ps. Having established that neither the hydrated electrons nor the OH radical possess rotational anisotropy, we infer that any rotational anisotropy measured at 193 nm pertains to ground state OH^-. Figure 4b shows the rotational anisotropy measured at 193 nm. Apart from an initial spike reminiscent of the $t = 0$ peaks, the rotational anisotropy grows to a maximum of $r(2\ \text{ps}) = 0.2$ followed by an exponential decay with a 1.9 ps time constant. It appears from Figure 4b, that the initial value of the anisotropy falls short of the value of $r(0) = 0.4$ characteristic of the orientation anisotropy created by preferential depletion of an isotropic distribution. The rotational anisotropy is modeled and discussed in section 5b.

5. Discussion

5a. Modeling the Photodetachment. On the basis of the detachment dynamics outlined in the introduction, we have modeled the photodetachment with the purpose of verifying the assignments in section 4, modeling the quantum yields of the photodetachment process and, hopefully, providing new insight into the detachment process, in particular the CTTS state and the hot $(OH^-)^*$ molecules responsible for the additional transient absorption observed at short delays below 220 nm.

To successfully describe the temporal dynamics of the data, the model must describe both the bimodal recombination dynamics of the OH and e^- detachments products and the spectral dynamics caused by the hot $(OH^-)^*$ ion relaxing toward the ground state of OH^-. We have modeled the recombination dynamics by directly solving the diffusion equation for a pair of reactants moving under the influence of a weak potential.[43]

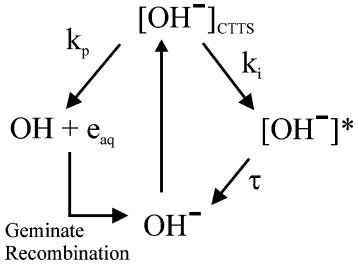

Figure 5. Model of the reaction dynamics following excitation of OH^- at 200 nm.

The diffusive recombination dynamics of the detachment products is combined with a simple rate equation describing the excitation into the CTTS state and the subsequent decay of the CTTS state into either the detachment products, OH and e^-, or into the hot $(OH^-)^*$ ions. In Figure 5 we have illustrated the simple model described by the rates k_p and k_i for the two decay channels of the CTTS state, and the relaxation time τ of the hot $(OH^-)^*$ ions. The geminate $OH-e^-$ pairs subsequently recombine at a rate given by the numerical solution to the diffusion equation. The inclusion of the attractive potential in the diffusive motion of the detachment products is equivalent to the inclusion of a contact-pair $OH-e^-$. In line with Crowell et al.[8] we note that the temporal dynamics of the recombination process cannot be modeled with free diffusion, consistent with the presence of a contact pair. Once the diffusive dynamics have been calculated we calculate the transient spectra, by multiplying the steady-state spectra of OH^-, OH, and e^-, in stochiometric proportions, with the time evolution of their concentrations. With the wide range of probe wavelengths, this provides a restrictive test of the consistency of the kinetic model used.

The recombination dynamics can be determined from either the 270 nm data or the 800 nm data, shown in Figure 2c and 2d. Only the OH radical and the hydrated electron contribute, and, if normalized, the time evolution of the two data sets is exactly the same. The recombination dynamics depend on the diffusion coefficients and the reaction radii of the two fragments, OH and e^-. We adopt the values $D = D_{OH} + D_{e^-} = 7 \times 10^{-9}$ $m^2\ s^{-1}$ and $R_{eff} = 0.56$ nm from the works of Elliot et al.[44] and Crowell et al.[8] Inspired by previous work,[8,45] we use a simple Morse potential, with an Onsager length of 0.7 nm and a potential depth of 2.5 kT at $R = 0.3$ nm. Finally we need to specify the pair distribution function at $t = 0$, $p(r)$, describing the location of the two fragments at the onset of the diffusive recombination. We have chosen an exponential distribution, that decays rapidly from $r = R_{eff,}$ with a $1/e$ length of 0.125 nm.

$$p(r) = \exp((r - R_{eff})/L) \tag{2}$$

where $r \geq R_{eff} = 0.56$ nm, $L = 0.125$ nm.

$$p(r) = 0 \tag{3}$$

where $r \leq R_{eff}$.

These parameters are very similar to the set of parameters used by Crowell et al.[8] We note that recombination dynamics can be modeled with a variety of assumed potentials, pair distribution functions, and reaction radii, and the numerical procedure does not warrant a determination of any of these parameters, as was also noted by Crowell et al.[8] However, using plausible values and values determined from other investigations,[44] we obtain good agreement between model and experimental data. This is illustrated in Figure 2c where the recombination dynamics obtained directly from solving the diffusion equation is shown as a dotted line on top of the experimental

data. The finite rise time of the model is caused by the lifetime of the CTTS state, which we will discuss shortly. The influence of the nonvanishing pair potential, $V(r)$, can be viewed by looking at the transient data at 270 nm, where only the OH and e^- products contribute to the transient absorption signals (see Figure 2c). We have numerically removed the coherence spike at $t = 0$ in the 270 nm experimental data before comparing them to the numerical solution to the diffusion equation (not shown in the figure). Once the potential is turned of, $V(r) = 0$, the agreement with the data rapidly deteriorates. Modeling the recombination dynamics using a numerical solution to the diffusion equation is equivalent to the model used by Crowell et al.[8] Here the analytical expression given by Shushin[46−48] models the recombination by explicitly considering the recombination and dissociation rate of the contact pair, W_r and W_d. The fast component of the recombination is thus a consequence of contact pair recombination, whereas the slower part of the recombination is a consequence of contact pair dissociation followed by free diffusive recombination. In our numerical simulation, the ratio between fast and slow recombination is determined, assuming a fixed reaction rate, by separation of the fragments at $t = 0$, expressed by the location of the exponential pair distribution function and the strength of the interpair potential.

We obtain good agreement with the experimental observations by setting $k_i = 6\ ps^{-1}$ and $k_p = 11\ ps^{-1}$ corresponding to a CTTS state lifetime of $\tau_{CTTS} = (k_p + k_i)^{-1} < 100$ fs. Given the pump pulse duration of 200 fs, we cannot attribute any significance to the absolute value of these rates, and the underlying physical mechanism pertaining to the CTTS state. However, the ratio of the two rates, $QY_{CTTS} = k_p/(k_p + k_i) = 0.65$, corresponding to the quantum yield for dissociation of the CTTS state, is important for the extraction of the spectral characteristics of the relaxing hot $(OH^-)^*$ molecules.

As seen from Figure 3 only OH^-, OH, and e^- contribute to the transient signals at delays longer than 5 ps. We can consequently use the recombination dynamic obtained from the 800 nm data, to describe the entire transient spectrum from 193 nm to 800 nm. By scaling the time evolution of the recombination dynamics with the known steady-state spectra of OH^-, OH, and e^-, we can describe the transient spectrum at delays longer than 5 ps, and we are also able to obtain more information on the additional spectral dynamics observed at delays shorter than 5 ps from 193 to 220 nm. The additional transient absorption at short delays is obtained by subtracting the OH^-, OH, and e^- contributions, scaled by the recombination dynamics. In Figure 6 the experimental data from 193 to 216 nm are shown as points and the transient absorption obtained from multiplying the steady-state spectra of OH^-, OH, and e^- is shown as dotted lines. Two things are evident from Figure 6. First of all the transient spectra for delays longer than approximately 5 ps are well described by the recombination dynamics inferred from the 800 nm data. In fact, the entire transient spectrum from 193 to 800 nm is well described by this simple recombination of OH and e^- and subsequent recovery of the bleaching of OH^-. There are small deviations concerning the amplitude of the transient absorption at individual probe wavelengths, for example at 200 nm, but we believe that this is a result of the uncertainties pertaining to the steady-state spectra and the overlap procedure used to bring the individual probe scans on a common wavelength scale. Second, it is also evident that for delays shorter than 5 ps, there is a significant additional contribution to the transient absorption. The additional transient absorption is largest at small wavelengths close to the OH^- absorption peak and then gradually decays as the probe wavelengths increases. This is also seen in the contour plot in Figure 3, where rapid spectral changes are observed at delays shorter than 5 ps. Above 220 nm there is no additional absorption and the entire transient spectrum is for all delays accurately modeled by scaling the recombination dynamics with the steady-state spectra. From the difference between the observed and the modeled transient absorption, we can obtain a transient spectrum of the alleged contribution from $(OH^-)^*$. Guided by the shape of the ground state OH^- spectrum, we have for each delay fitted the residual transient spectrum by a Gaussian described by a center wavelength, width, and amplitude. Consequently, the full model depicted in Figure 6 does not completely reproduce the experimental data. However, the agreement between model and experiment is much improved, and we obtain a time-dependent spectrum of the hot $(OH^-)^*$ molecules, shown in Figure 7. The spectrum resembles that of a vibrationally relaxing molecule, showing an increased absorption toward lower energy at short delays which rapidly converges toward the steady-state OH^- spectrum.[41] After approximately 2−3 ps, the hot $(OH^-)^*$ molecules have all returned to the ground state of OH^-. For excited OH^-, both vibrational and electronic degrees of freedom are strongly coupled to the solvent and we do not expect to be able to describe the relaxation as a purely intramolecular conversion process followed by vibrational relaxation of OH^- through intermolecular solvent modes. We find it more likely that the conversion of the electronic excitation energy is mediated by the intermolecular solvent coordinates, i.e., by a rapid rehydration of $(OH^-)^*$ to form ground state OH^-. In other words the vibrational relaxation observed is relaxation in both the solvent coordinates and the OH^- vibration

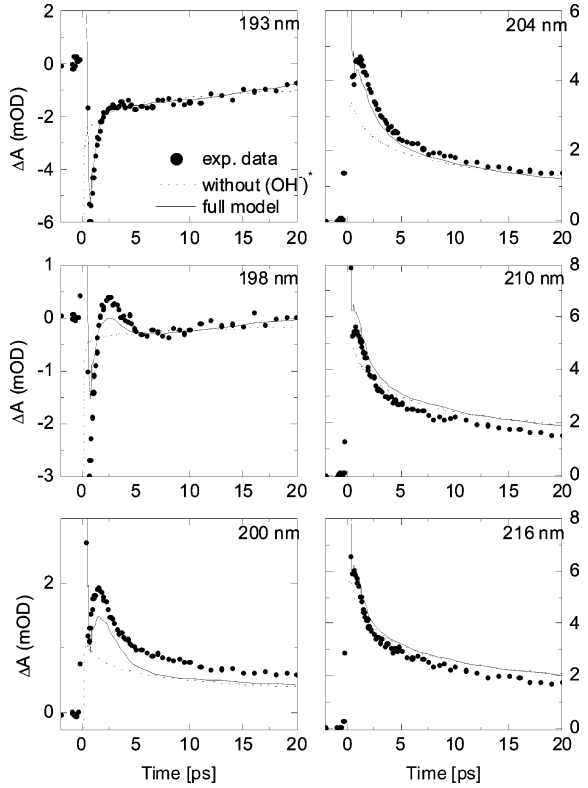

Figure 6. Comparison of measured (dotted curve) and modeled (line) transient absorption traces at selected wavelengths between 193 and 216 nm.

Given the very fast vibrational energy lifetime of the O−H stretch in water[49] of ∼200 fs, and the equally fast redistribution

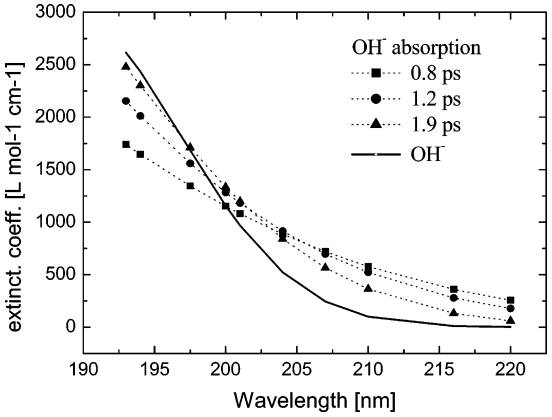

Figure 7. Experimental spectra of the hot $(OH^-)^*$ molecules af 0.8, 1.2, and 1.9 ps. The full line corresponds to the equilibrium OH^- absorption spectrum. The observed increase in absorption at larger wavelengths and the decreasing absorption at shorter wavelengths are in accordance simple models describing a non- or partly hydrated OH^- molecule.

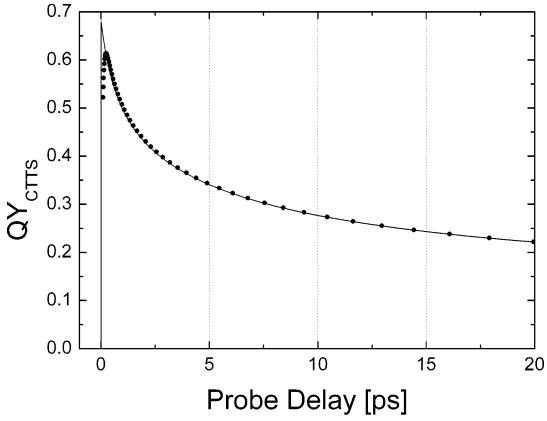

Figure 8. Quantum yield of OH and e^- as a function of time obtained from the model presented in Figure 5 with the parameters given in section 5b.

of vibrational energy among the low-frequency intermolecular modes in water,[50] we cannot determine to what extent the electronic energy is accepted directly by the solvent modes or indirectly through excitation of the OH^- vibration and subsequent dissipation to the solvent modes.

Assuming that the solvent coordinates in play are primarily associated with the hydrogen bonds to and from OH^-, we obtain a rudimentary idea about the spectra of nonhydrated OH^- from studies of heated solutions of OH^-. Since the number of intact hydrogen bonds drop with increasing temperature, a nonhydrated state of OH^-, i.e. a state with fewer hydrogen bonds connecting water and OH^- can qualitatively be studied by observing the CTTS absorption spectrum as a function of temperature. This shows that the absorption maximum shift toward longer wavelength as the temperature is increased, and the spectral width remains nearly constant.[4] From the spectrum depicted in Figure 7 we see that the equilibration of hot $(OH^-)^*$ results in a fast blue-shift of the CTTS band. Initially, the solvent molecules close to the hot $(OH^-)^*$ are in a nonequilibrium geometry, resulting in a red-shifted CTTS band. As this nonequilibrium condition relaxes, the energy being dissipated by the water solvent, the CTTS band blue shifts toward is equilibrium position.

Naturally, using a spectrum based on the observed residuals, we obtain a very good agreement between the experimental data and the model. As seen in Figure 6, the agreement at 193, 198, and 200 nm shows that the model convincingly handles the 2 ps absorption recovery caused by solvent-assisted conversion and recombination of $OH-e^-$ pairs, in addition to the contributions from the formation of hydrated electrons and OH radicals occurring within the first 0.3 ps. The spectrum of hot $(OH^-)^*$ decays in approximately 2 ps. As the rehydration of hot $(OH^-)^*$ involves reorientation of the hydrogen bonds[51] of the first hydration shell, and as this again provides the necessary coupling to relax the electronic energy of hot $(OH^-)^*$, a picosecond spectral relaxation time is expected corresponding to the rotational motion taking place.

As noted earlier, changes in the initial quantum yield for dissociation of the CTTS state, $QY_{CTTS} = k_p/(k_p + k_i)$ will influence the shape and amplitude of the spectrum of the hot $(OH^-)^*$ molecules. The time-dependent quantum yield obtained from the recombination dynamics is shown in Figure 8. The full line is the recombination dynamics obtained from solving the diffusion equation as described earlier, and the points correspond to the dynamics after taking into account the finite width of the 200 nm pump pulse and the life time of the CTTS state. The crucial point is the extrapolation of the quantum yield to $t = 0$. From our analysis we obtained a quantum yield of $QY(t \rightarrow 0) = 65 \pm 5\%$. The quantum yield after 5 ps is in good agreement with the findings of Crowell et al.,[7] who determined photodetachment quantum yield, based on the measured electron concentration after 5 ps and used a biexponential fit to estimate a prompt yield of $QY(t \rightarrow 0) = 37\%$. This is about a factor of 2 lower than the estimate derived from our model. The discrepancy seems surprising since all quantum yields after five ps are in full agreement and the absorption dynamics of the first 5 ps are identical in the two studies. However, extrapolating the recombination dynamics to $t = 0$ is not trivial, as limitations in the time resolution, the coherence spikes at $t = 0$, and rapid changes in the spectrum of the hydrated electron during the first 2 ps[21] can influence the extrapolation. So the determination of the $QY(t \rightarrow 0)$ will be highly model-dependent. Also the quantum yield obtained at long delays, $t = 200$ ps is in agreement with those reported by Dainton and Fowles,[15] Iwata et al.,[16] and Crowell et al.[7]

A distinct feature in our model is the assumption that a relative large fraction of the excited CCTS states, ~35%, are converted into a population of hot $(OH^-)^*$ molecules. In our view this is different from the immediate/fast recombination of close lying pairs of OH and e^-. We do observe fast recombination caused by recombination of closely lying geminate partners, but this does not result in the characteristic spectral evolution observed between 200 and 220 nm. Similarly, we do not observe spectral transients following the recombination taking place at delays beyond 20 ps. To further investigate the possible presence of hot $(OH^-)^*$ molecules, we have examined alternative reaction schemes. In particular, we have assessed the importance of the solvent-assisted conversion channel, by omitting it from the model and instead assuming a spectral relaxation of the OH^- molecules formed through the geminate recombination $OH + e^-$. To do this we adopt a simple model for the relaxing OH^- molecules, based on a temperature-dependent red shift of the equilibrium OH^- CTTS band, described by a simple Gaussian line shape.[4] We test three specific scenarios: (a) the model described above, where hot $(OH^-)^*$ are formed exclusively through solvent-assisted conversion, (b) a model where the hot $(OH^-)^*$ molecules are exclusively formed from geminate recombination recombined, and (c) a model where hot $(OH^-)^*$ molecules are formed through both mechanisms. In each case, we optimize the spectral red shift to achieve the best agreement with the data. Model a reproduces the experimental spectra quite

accurately, whereas models b and c cannot reproduce the observed transients. We therefore conclude that no spectral relaxation of OH^- is present after geminate recombination of OH and e^-, whereas a substantial spectral relaxation takes place in the solvent-assisted conversion of the CTTS state. The main reason for the difference between hot $(OH^-)^*$ molecules formed from solvent-assisted conversion of the CTTS state and OH^- molecules formed through geminate recombination of OH and e^- is the amount of electronic energy that must be dissipated. The detachment energy of OH^- is approximately 6.6 eV in water. However, geminate recombination takes place between hydrated fragments, and a significant part of the detachment energy is thus dissipated as hydration energy of the two fragments. Thus, upon recombination the amount of energy that must be dissipated is lower than the detachment energy. In terms of solvent configurations this is equivalent to stating that the combined hydration shells of the two fragments closely resemble that of the hydrated OH^- molecule. On the other hand, the fraction of CTTS states that return directly to the alleged hot $(OH^-)^*$ could do so without the fragments actually being separated. Consequently, this would leave almost all the detachment energy to be dissipated by the solvent-assisted conversion process involving coupling to the nearest solvent molecules. We note that the relaxation time of the spectral signatures attributed to hot $(OH^-)^*$ is ~2 ps in good agreement with typical solvent reorientation time in water.[51,52] A related mechanism in aqueous ions has been studied by nonadiabatic quantum molecular dynamics simulation by Sheu and Rossky.[6] They studied the details of the photodetachment process and showed that two distinct processes are active: A direct photodetachment process (DP), where the electron is ejected directly into a preexisting cavity in the solvent, and an indirect process (CP) where the electron first relaxes through the manifold of CTTS states to a state of predominantly s-character, which then is ejected into the solvent as soon as a nearby cavity is formed through solvent fluctuations. From these simulations, one could speculate that the fast conversion of the CTTS state into hot $(OH^-)^*$ molecules is related to the CP channel.

Our experimental results also confirm the existence of a OH^- e^- contact pair, or equivalently, show that an attractive potential between OH and e^- is needed to account for the recombination dynamics. As noted in the work of Crowell et al.,[8] the activation energy of the dissociation for the contact pair is nearly equal to that of the diffusion coefficient for the solvated electron. Furthermore, the spectral characteristics for both OH and e^- are unchanged in the contact pair, so perhaps one should rather speak of a preferred proximity of the two free entities OH and e^-, i.e. a slight enhancement in the amplitude of the pair distribution function of the two. This was inferred earlier in the case of the $NO_3^- + H^+$ distribution in water,[53] where the protons tend to localize closer to the parent anion. In other words the term "contact pair" might suggest a structure far more rigid and stable than actually observed in the experiments and inferred from the different models employed.

The good agreement with experimental data also provides valuable information about the spectra utilized in the model. The calculated transient spectra depend somewhat on the choice of OH absorption spectrum. Using the absorption spectrum of OH reported by Boyle et al.[22] instead of that published by Thomsen et al.[20,21] yields spectral dynamics in fair agreement with the data above 210 nm but fails to reproduce the absorption at shorter wavelength, reflecting the much lower absorption of OH below 210 nm. The model may also be used to test the validity of the ultraviolet part the hydrated electron spectrum. The far-UV spectral part of the hydrated electron has only been measured by Nielsen et al.[30] The measured extinction coefficient decreases monotonously from 700 to 210 nm but then increases below 210 nm. Detailed analysis of our data shows that omitting this increase results in a significantly poorer agreement with our data.

In summary, the analysis of the temporal dynamics of the transient spectra supports the notion of a contact pair, and the spectral analysis shows the presence of an additional absorbing transient other than OH^-, OH, and e^-. We assign this transient to hot $(OH^-)^*$ molecules formed through solvent-assisted conversion immediately after the photodetachment. In section 5c we will further discuss the properties of this state in light of a series of *ab initio* calculation of microhydration of OH^-.

5b. Modeling the Rotational Anisotropy. In aqueous solution OH^- is bonded to on average 3−5 of the surrounding water molecules.[54−56] OH^- has an unusually high diffusion coefficient of ~5 $Å^2$/ps because it moves through the solvent by rapid structural diffusion, involving the constant breaking and formation of intramolecular O−H bonds and hydrogen bonds and slight changes in the electron densities (the Grotthuss mechanism[57]). The diffusion is accompanied by rapid reorientation. The structure and mobility mechanism of OH^- have been investigated recently using Car—Parrinello molecular dynamics (CPMD) calculations. Tuckerman et al.[54,55,58] showed how OH^- is predominantly solvated in a planar $[OH^-,4H_2O]$ structure in which the oxygen atom is coordinated by hydrogen bonds to four water molecules, each pointing one O−H bond toward the oxygen atom. The O−H bond of OH^- is approximately perpendicular to the plane of the hydrogen bonds. Solvent fluctuations may break one of the hydrogen bonds thereby enabling the formation of the less stable tetrahedral $[OH^-,3H_2O]$ complex. Transitions between the two structures are accompanied by a substantial reorientation of OH^-. Still following the calculations by Tuckerman et al., no significant diffusion of OH^- occurs while it is in the $[OH^-,4H_2O]$ structure, whereas the $[OH^-,3H_2O]$ complex diffuses several intermolecular distances in a matter of 1 ps. Including the K^+ counterion in the CPMD calculations reveals the additional hydration structure of $[OH^-,5H_2O]$.[59,60] The calculations including the K^+ cation further indicate that diffusion occurs in the $[OH^-,3H_2O]$ and $[OH^-,4H_2O]$ structures but not in the $[OH^-,5H_2O]$ complex. Since transitions between the two structures and diffusion are accompanied by reorientation of the OH^-, the rotational anisotropy measurements reflect the time spent in the $[OH^-,4H_2O]$ and $[OH^-,3H_2O]$ complexes. Recent simulations by Laage and Hynes[52] of Cl^- in water also indicates a strong coupling between reorientational and translational motion of the water molecules in the first and second solvation shell surrounding the halide ion.

If only one species contributes to the absorption at a specific wavelength eq 1 gives the rotational anisotropy. It follows from eq 1 that $r(t)$ is either positive or negative and assumes a maximum of $|r(t = 0)| = 0.4$. When more than one species contributes to the transient absorption, eq 1 generalizes to:

$$r'(t) = \frac{\sum_i (\Delta A_{\parallel}^i - \Delta A_{\perp}^i)}{\sum_i (\Delta A_{\parallel}^i + 2\Delta A_{\perp}^i)} \qquad (4)$$

Here the summation runs over every absorbing species. $r'(t)$ behaves very differently from that of eq 1. For instance, even species with no rotational anisotropy affect $r'(t)$ by contributing

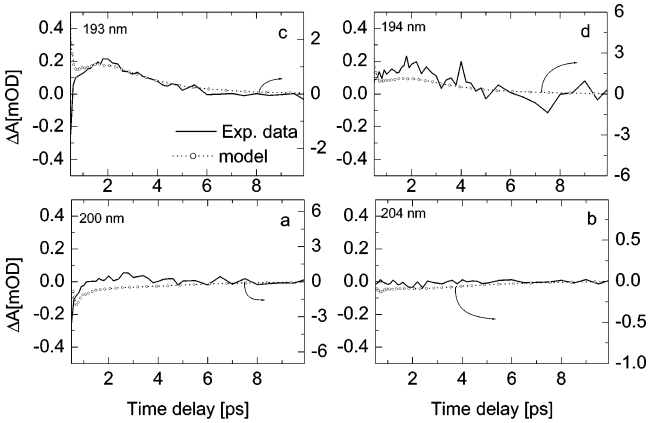

Figure 9. Rotational anisotropy measurements compared to anisotropies calculated using eq 2 in conjunction with the model schematically shown in Figure 5.

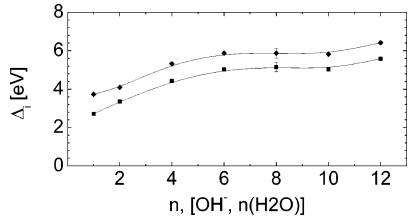

Figure 10. Energies of excited states of $[OH^-,nH_2O]$ calculated at the CIS(D)/ AUG-cc-pVDZ level of theory. ♦ and ■ indicate excited states 1 and 4, respectively. The error bars in case of $n = 8$ are estimated from three $[OH^-,nH_2O]$ conformations where the number of hydrogen bonds involving OH^- is 5, 4, and 3, respectively. The full lines are drawn as a guide to the eye.

to the denominator, and species having transient absorptions of opposite signs result in a maximum of $r'(t)$, which is very different from $r(t = 0) = 0.4$, and the maximum can occur at times later than $t = 0$. The maximum value of $r'(t)$ may even approach infinity if the total transient absorption approaches zero. In the rotational anisotropy measurement at 193 nm depicted in Figure 4b, the reduced and late appearance of the $r'(t)$ maximum reflects the contributions to $r'(t)$ from hydrated electrons and hydroxyl radicals. In order to obtain a more accurate description of the rotational anisotropy of OH^-, we have measured $r'(t)$ at a number of wavelength around 200 nm. The results are depicted in Figure 9. The figure also shows $r(t)$ calculated on the basis of the model depicted in Figure 5. In some of the figures the amplitude of the calculated $r'(t)$ is scaled to fit the measured $r(t)$. The calculated amplitudes of $r'(t)$ are shown on the right-hand axis of each figure. Apart from the scaling factor, the only free parameter is the reorientation time of OH^-. The best overall agreement between the measured and calculated curves is achieved with a reorientation time of $\tau =$ 1.9 ps. The calculated curves are in good qualitative agreement with the measurements. The reorientation time is also similar to the spectral relaxation time deduced from the transient absorption pertaining to the hot $(OH^-)^*$ discussed earlier. However, the calculated amplitudes of the rotational anisotropy are significantly off. This deviation is at least in part due to the very strong wavelength dependence of the OH^- absorption together with the fact that the finite spectral width of the femtosecond probe pulses measures an average of $r(t)$ over 2−3 nm, which reduces the observed amplitudes relative to the calculated values.

The reorientation time of 1.9 ps certainly agrees with the timescales expected for diffusive reorientation.[51] Although exact diffusion coefficients cannot be deduced from the work of Tuckerman et al.,[54] the combination of their calculated mean square displacement of OH^- and the 1.9 ps reorientation time indicates that on average OH^- hardly stays in the $[OH^-,4H_2O]$ configuration for more than 2 ps. On the other hand, if OH^- were to stay in the $[OH^-,3H_2O]$ structure for more than 1 ps at a time, the reorientation time would likely be shorter than the observed 1.9 ps. It is informative to compare the reorientation time for the dilute concentrations of OH^- measured in the present work to the reorientation of OH measured in highly concentrated solutions of NaOX (X = H, D). Using infrared pump−probe spectroscopy Nienhuys et al.[61] have studied the rotational reorientation of the OH group in 10 M solutions of NaOX (X = H, D). These measurements revealed a very slow (and undetermined) decay in the rotational anisotropy indicating very rigid solvent−solute structure in which OH is only allowed small angular movements. Nienhuys et al. assigned the rigid, "gel-like" nature of the hydrogen bond network to the high charge density of the 10 M solution. The rotational anisotropy of 40 mM aqueous hydroxide presented here shows that structural diffusion enables OH^- to rotate much more freely at low concentrations. As mentioned earlier, very recent work by Laage and Hynes[52,62] suggests that the standard notion of diffusive reorientation of water molecules should be replaced by a molecular jump mechanism, where reorientation of a hydrogen-bonded water molecule takes place through a large angular jump of ∼60° preceded by an overcoordinated *transition state* where the hydrogen bond is bifurcated. Interestingly, they find that the H-bond reorientation mechanism is the same for both the water−water system and the investigated water−chloride system. The present measurement of the rotational anisotropy at 193 nm pertain to the ground state of the hydroxide ion in an equilibrated hydration sphere. The measurements are therefore unbiased in terms of which H-bonds are probed and provides a good estimate of the reorientation time of the hydrogen-bonded OH^-. The simulation gives a reorientation time for a water molecule H-bonded to chloride of 2.2 ps and 2.6 for the water−water H-bond. This is in agreement with the reorientation time of the hydroxide ion of 1.9 ps obtained in this work, although one could have argued, that it should have been slightly larger to conform to the notion that chloride is a weak structure breaker and hydroxide is a weak structure maker, which should reflect in the value of the reorientation times.

Since the rotational relaxation time of OH^- is about a factor of 5 longer than the upper limit for the lifetime of the CTTS state, it might be expected that the orientation of OH^- is transferred to the solvated OH radical after detachment of the electron. The lack of rotational anisotropy at 260 nm shows that this is not the case. Hence, the orientation of OH^- is either lost in the CTTS state, in the contact pair or by reorientation of the solvated OH radical in less than 0.3 ps after detachment from the electron. According to Car—Parrinello molecular dynamics simulations, the OH radical is on average bonded to 2.56 water molecules by hydrogen bonds with an average lifetime of ∼0.7 ps.[63] Moreover, the hydrogen bonds between the water molecules have a lifetime of ∼0.9 ps. Following these calculations, it therefore seems unlikely that the orientation of OH is lost in 0.3 ps by diffusive reorientation. In contrast, classical molecular dynamics simulations indicate that the OH radical may very well lose its anisotropy by diffusion.[64] Thus, in the most frequent structure, OH has one water molecule bound to the oxygen atom (O_2H_3) and one water molecule bound to the hydrogen atom (H_3O_2) in addition to the less frequent structures O_3H_5 and O_4H_7. The lifetimes of these structures are all less than 40 fs, giving the OH radical plenty of time to

TABLE 1: Calculated Excitation Energies, $\Delta_1 = E_1 - E_0$, from the Ground State to the First Excited-State in the Complex, [OH, $n$$H_2O$] Using the Cis(D) Method with Various Basis Sets

basis set	Δ_1, eV
311+G(d,p)	5.61
311++G(d,p)	3.02
aug-cc-pvdz	2.71
aug-cc-pvtz	2.78
aug-cc-pvqz	2.81

reorient. Still, the OH radical may also lose its orientation in the CTTS state or the contact pair prior to hydration.

5c. Theoretical Investigations. To gain further insight into the spectral evolution of hot $(OH^-)^*$ molecules, we have performed a series of simple *ab initio* electron structure calculations of the ground and excited states in gaseous clusters of OH^- and n water molecules, [OH^-, nH_2O] ($n \leq 12$). The level of calculation is the CIS(D) method,[65,66] which is applied to [OH^-, nH_2O] in a potential minimum obtained at the B3LYP/6-311+G(d,p) level. The electronic excitation energies from the ground state to the excited states are calculated assuming the [OH^-,nH_2O] structures are the same in the various states. CIS-(D) calculations on anions require large basis sets as illustrated in Table 1, which lists the first excitation energy, Δ_1, for [OH^-, $1H_2O$] obtained with various basis sets. The table shows a large variation of Δ_1. In particular, it is instructive to note the dramatic change in Δ_1 by addition of diffuse functions to the hydrogen atoms (i.e., replacing 6-311+G(d,p) by 6-311++G(d,p)). Guided by this table we have chosen the aug-cc-pvdz basis set for the calculation of excitation energies. This choice represents a balance between a fairly large basis set and the practical possibility to investigate clusters that have a maximum of hydrogen bonds involving OH^- as well as several solvent molecules not directly bound to OH^-.

Figure 10 shows the excitation energies for a few of the excited [OH^-, nH_2O] states. As n is increased, the excitation energy rapidly converges toward the range of the CTTS band observed in bulk water. Whereas the Δ_1-transition depends critically on n, the different excited states show more or less similar n-dependence. This suggests that the excited OH^- states are very diffuse states[67] resembling dipole bound states,[17] where a free charge is bound by the core dipole moment. In this case, the dipole moment is the static OH^- dipole moment, and induced dipole moment from the oriented water molecules close by. As the excited states are very diffuse, they probe a much larger configuration space of solvent molecules and they are less prone to be influenced by the specific solvent configuration, as opposed to the OH^- ground state. The number of water molecules, n, can also be interpreted as a way to describe the degree of hydration of the OH^- molecule. Low n-number thus indicates incomplete hydration. The large red-shift of the Δ_1-transition with decreasing n is consequently in good agreement with the assignment of the hot $(OH^-)^*$ transient absorption, rapidly blue shifting as a consequence of the rapid rehydration of OH^-.

6. Conclusion

In summary, we have investigated the photodetachment of OH^- at 200 nm. The experimental data indicate two primary reaction channels. The hydroxide ion, OH^-, is excited to the CTTS state from which 62% of the molecules detach to form an OH:e^- contact pair and 38% return to the ground state via solvent-assisted conversion, giving rise to hot (OH^-) molecules observed in the first ~4 ps below 220 nm. The combined rate of solvent-assisted conversion and contact pair formation depopulates the CTTS state in less than 0.4 ps. The contact pairs, or rather two separated OH and e^- fragments diffusing under the influence of a weakly attractive potential, recombine geminately, leaving a quantum yield of OH radicals of 13% after 200 ps in good agreement with previous work with lower time resolution. Rotational anisotropy measurements of OH^- and OH give an OH^- reorientation time of $\tau = 1.9$ ps and further show that the rotational anisotropy of OH^- is not transferred to the OH radical, which is isotropic 0.3 ps after the excitation.

References and Notes

(1) Schulz, P. A.; Mead, R. D.; Jones, P. L.; Lineberger, W. C. *J. Chem. Phys.* **1982**, *77* (3), 1153−1165.

(2) Smith, J. R.; Kim, J. B.; Lineberger, W. C. *Phys. Rev. A* **1997**, *55* (3), 2036−2043.

(3) Winter, B.; Faubel, M.; Hertel, I. V.; Pettenkofer, C.; Bradforth, S. E.; Jagoda-Cwiklik, B.; Cwiklik, L.; Jungwirth, P. *J. Am. Chem. Soc.* **2006**, *128* (12), 3864−3865.

(4) Fox, M. F.; McIntyre, R.; Hayon, E. *Faraday Discuss.* **1977**, *64*, 167−172.

(5) Sander, M. U.; Luther, K.; Troe, J. *Ber. Bunsen-Ges.* **1993**, *97* (8), 953−961.

(6) Sheu, W. S.; Rossky, P. J. *J. Phys. Chem.* **1996**, *100* (4), 1295−1302.

(7) Crowell, R. A.; Lian, R.; Sauer, M. C.; Oulianow, D. A.; Shkrob, I. A. *Chem. Phys. Lett.* **2003**, *383*, 481−485.

(8) Crowell, R. A.; Lian, R.; Shkrob, I. A.; Bartels, D. M.; Chen, X. Y.; Bradforth, S. E. *J. Chem. Phys.* **2004**, *120* (24), 11712−11725.

(9) Iglev, H.; Laenen, R.; Laubereau, A. *Chem. Phys. Lett.* **2004**, *389* (4−6), 427−432.

(10) Assel, M.; Laenen, R.; Laubereau, A. *Chem. Phys. Lett.* **1998**, *289* (3−4), 267−274.

(11) Sauer, M. C.; Crowell, R. A.; Shkrob, I. A. *J. Phys. Chem. A* **2004**, *108* (25), 5490−5502.

(12) Sauer, M. C.; Shkrob, I. A.; Lian, R.; Crowell, R. A.; Bartels, D. M.; Chen, X. Y.; Suffern, D.; Bradforth, S. E. *J. Phys. Chem. A* **2004**, *108* (47), 10414−10425.

(13) Lian, R.; Oulianov, D. A.; Crowell, R. A.; Shkrob, I. A.; Chen, X. Y.; Bradforth, S. E. *J. Phys. Chem. A* **2006**, *110* (29), 9071−9078.

(14) Moskun, A. C.; Bradforth, S. E.; Thogersen, J.; Keiding, S. *J. Phys. Chem. A* **2006**, *110* (38), 10947−10955.

(15) Dainton, F. S.; Fowles, P. *Proc. R. Soc. London, Ser. A:* **1965**, *287* (1410), 312.

(16) Iwata, A.; Nakashima, N.; Kusaba, M.; Izawa, Y.; Yamanaka, C. *Chem. Phys. Lett.* **1993**, *207* (2−3), 137−142.

(17) Robertson, W. H.; Johnson, M. A. *Annu. Rev. Phys. Chem.* **2003**, *54*, 173−213.

(18) Ronne, C.; Keiding, S. R. *J. Mol. Liq.* **2002**, *101* (1−3), 199−218.

(19) Pagsberg, P.; Christen, H.; Rabani, J.; Nilsson, G.; Fenger, J.; Nielsen, S. O. *J. Phys. Chem.* **1969**, *73* (4), 1029.

(20) Thomsen, C. L.; Madsen, D.; Keiding, S. R.; Thogersen, J.; Christiansen, O. *J. Chem. Phys.* **1999**, *110* (7), 3453−3462.

(21) Madsen, D.; Thomsen, C. L.; Thogersen, J.; Keiding, S. R. *J. Chem. Phys.* **2000**, *113* (3), 1126−1134.

(22) Boyle, J. W.; Ghormley, J. A.; Hochanad, C. J.; Riley, J. R. *J. Phys. Chem.* **1969**, *73* (9), 2886.

(23) Czapski, G.; Dorfman, L. M. *J. Phys. Chem.* **1964**, *68* (5), 1169.

(24) Alam, M. S.; Janata, E. *Chem. Phys. Letters* **2006**, *417* (4−6), 363−366.

(25) Janik, I.; Bartels, D. M.; Jonah, C. D. *J. Phys. Chem. A* **2007**, *111* (10), 1835−1843.

(26) Lian, R.; Crowell, R. A.; Shkrob, I. A. *J. Phys. Chem. A* **2005**, *109* (8), 1510−1520.

(27) Saeki, A.; Kozawa, T.; Tagawa, S. *Nucl. Instrum. Methods Phys. Res., Sect. A:* **2006**, *556* (1), 391−396.

(28) Jou, F. Y.; Freeman, G. R. *J. Phys. Chem.* **1979**, *83* (18), 2383−2387.

(29) Baltuska, A.; Emde, M. F.; Pshenichnikov, M. S.; Wiersma, D. A. *J. Phys. Chem. A* **1999**, *103* (49), 10065−10082.

(30) Nielsen, S. O.; Pagsberg, P.; Hart, E. J.; Christen, H.; Nilsson, G. *J. Phys. Chem.* **1969**, *73* (9), 3171.

(31) Nielsen, S. O.; Michael, B. D.; Hart, E. J. *J. Phys. Chem.* **1976**, *80* (22), 2482−2488.

(32) Shkrob, I. A.; Glover, W. J.; Larsen, R. E.; Schwartz, B. J. *J. Phys. Chem. A* **2007**, *111* (24), 5232−5243.

(33) Madsen, D.; Larsen, J.; Jensen, S. K.; Keiding, S. R.; Thogersen, J. *J. Am. Chem. Soc.* **2003**, *125* (50), 15571−15576.

(34) Petersen, C.; Thogersen, J.; Jensen, S. K.; Keiding, S. R. *J. Phys. Chem. A* **2006**, *110* (10), 3383−3387.
(35) Thomsen, C. L.; Madsen, D.; Keiding, S. R.; Thogersen, J.; Christiansen, O. *J. Chem. Phys.* **1999**, *110* (7), 3453−3462.
(36) Crowell, R. A.; Bartels, D. M. *J. Phys. Chem.* **1996**, *100* (45), 17940−17949.
(37) Nemukhin, A. V.; Grigorenko, B. L. *Chem. Phys. Lett.* **1997**, *276* (3−4), 171−176.
(38) Poulsen, J. A.; Thomsen, C. L.; Keiding, S. R.; Thogersen, J. *J. Chem. Phys.* **1998**, *108* (20), 8461−8471.
(39) Thomsen, C. L.; Thogersen, J.; Keiding, S. R. *J. Chem. Phys.* **2001**, *114* (9), 4099−4106.
(40) Tarnovsky, A. N.; Alvarez, J. L.; Yartsev, A. P.; Sundstrom, V.; Akesson, E. *Chem. Phys. Lett.* **1999**, *312* (2−4), 121−130.
(41) Elsaesser, T.; Kaiser, W. *Annu. Rev. Phys. Chem.* **1991**, *42* 83.
(42) Nibbering, E. T. J.; Elsaesser, T. *Chem. Rev.* **2004**, *104* (4), 1887−1914.
(43) Krissinel, E. B.; Agmon, N. *J. Comput. Chem.* **1996**, *17* (9), 1085−1098.
(44) Elliot, A. J.; Mccracken, D. R.; Buxton, G. V.; Wood, N. D. *J. Chem. Soc.,Faraday Trans.* **1990**, *86* (9), 1539−1547.
(45) Kloepfer, J. A.; Vilchiz, V. H.; Lenchenkov, V. A.; Chen, X. Y.; Bradforth, S. E. *J. Chem. Phys.* **2002**, *117* (2), 766−778.
(46) Shushin, A. I. *J. Chem. Phys.* **1992**, *97* (3), 1954−1960.
(47) Shushin, A. I. *J. Chem. Phys.* **1991**, *95* (5), 3657−3665.
(48) Shushin, A. I. *Chem. Phys. Lett.* **1985**, *118* (2), 197−202.
(49) Cowan, M. L.; Bruner, B. D.; Huse, N.; Dwyer, J. R.; Nibbering, E. T. J.; Chugh, B.; Elsaesser, T.; Miller, R. J. D. *Nature* **2005**, *434* 199−202.
(50) Ashihara, S.; Huse, N.; Espagne, A.; Nibbering, E. T. J.; Elsaesser, T. *J. Phys. Chem. A* **2007**, *111* (5), 743−746.
(51) Ronne, C.; Thrane, L.; Astrand, P. O.; Wallqvist, A.; Mikkelsen, K. V.; Keiding, S. R. *J. Chem. Phys.* **1997**, *107* (14), 5319−5331.
(52) Laage, D.; Hynes, J. T. *Proc. Natl. Acad. Sci. U.S.A.* **2007**, *104* (27), 11167−11172.
(53) Keiding, S. R.; Madsen, D.; Larsen, J.; Jensen, S. K.; Thogersen, J. *Chem. Phys. Lett.* **2004**, *390* (1−3), 94−97.
(54) Tuckerman, M.; Laasonen, K.; Sprik, M.; Parrinello, M. *J. Chem. Phys.* **1995**, *103* (1), 150−161.
(55) Tuckerman, M. E.; Marx, D.; Parrinello, M. *Nature* **2002**, *417* (6892), 925−929.
(56) Chaudhuri, C.; Wang, Y. S.; Jiang, J. C.; Lee, Y. T.; Chang, H. C.; Niedner-Schatteburg, G. *Mol. Phys.* **2001**, *99* (14), 1161−1173.
(57) Ludwig, R. *Angew. Chem., Int. Ed.* **2003**, *42* (3), 258−260.
(58) Tuckerman, M.; Laasonen, K.; Sprik, M.; Parrinello, M. *J. Phys. Chem.* **1995**, *99* (16), 5749−5752.
(59) Chen, B.; Ivanov, I.; Park, J. M.; Parrinello, M.; Klein, M. L. *J. Phys. Chem. B* **2002**, *106* (46), 12006−12016.
(60) Chen, B.; Park, J. M.; Ivanov, I.; Tabacchi, G.; Klein, M. L.; Parrinello, M. *J. Am. Chem. Soc.* **2002**, *124* (29), 8534−8535.
(61) Bakker, H. J.; Woutersen, S.; Nienhuys, H. K. *Chem. Phys.* **2000**, *258* (2−3), 233−245.
(62) Laage, D.; Hynes, J. T. *Science* **2006**, *311* (5762), 832−835.
(63) Khalack, J. M.; Lyubartsev, A. P. *J. Phys. Chem. A* **2005**, *109* (2), 378−386.
(64) Campo, M. G.; Grigera, J. R. *J. Chem. Phys.* **2005**, *123* (8).
(65) Gaussian 03, (2004) Revision C.02, M. J. Frisch et al.; Gaussian, Inc., Wallingford, CT.
(66) Headgordon, M.; Rico, R. J.; Oumi, M.; Lee, T. J. *Chem. Phys. Lett.* **1994**, *219* (1−2), 21−29.
(67) Bradforth, S. E.; Jungwirth, P. *J. Phys. Chem. A* **2002**, *106* (7), 1286−1298.